

**Tropospheric aerosol characterization:  
from GOME towards an ENVISAT perspective**

**Maria João Costa (1, 2), Marco Cervino (1), Elsa Cattani (1), Francesca Torricella (1),  
Vincenzo Levizzani (1), Ana Maria Silva (2)**

*(1)Institute of Atmospheric and Oceanic Sciences (ISAO-CNR)*

*Via Gobetti, 101, 40129 Bologna, Italy.*

*e-mail: mj.costa@isao.bo.cnr.it*

*(2)University of Évora*

*Dept. of Physics, Rua Romão Ramalho 59, 7000 Évora, Portugal.*

*e-mail: asilva@uevora.pt*

**ABSTRACT**

The interest in aerosol observations from satellite passive instrument is steadily increasing as a result of the better understanding of the key role played by aerosols within the climate system. Satellite instruments supply global observations for establishing the aerosol climatology and characterizing single aerosol events. Since the 1980s data from geostationary meteorological satellites, such as the Geostationary Operational Environmental Satellite (GOES) and METEOSAT, and the Advanced Very High Resolution Radiometer (AVHRR) polar orbiting instruments have allowed for monitoring the aerosol optical thickness (AOT) over the oceans. More recently, it has been shown that the knowledge of the aerosol spectral optical properties is equally needed to understand the interaction of solar and terrestrial radiation with aerosols, together with a better appreciation of the role of clouds and surface reflection. Satellite observation have thus been directed towards the retrieval of AOT together with absorption potential, scattering efficiency and angular dependence, that is the identification of the predominant aerosol type over the scene. The Global Ozone Monitoring Experiment (GOME), in particular, has proved instrumental for the detection and characterization of the aerosol load, by exploiting its spectral coverage and resolution. An algorithm to determine the aerosol size distribution, spectral refractive index and AOT from GOME spectral reflectance is presented. The method is based on a non-linear fitting model. In addition, AOT values and aerosol type parameters derived from the GOME operational aerosol product can provide information for the algorithm initialization. Some examples are shown. The combination of the aerosol properties retrieved from high spectral resolution measurements with higher temporal frequency data from METEOSAT geostationary satellites is also included as an effective strategy for monitoring large atmospheric aerosol events. The algorithm is planned to be used with ENVISAT-1 data from the SCanning Imaging Absorption SpectroMeter for Atmospheric Chartography (SCIAMACHY), the MEDium Resolution Imaging Specrometer (MERIS), and the Advanced Along Track Scanning Radiometer (AATSR). An overall improvement of the results is expected given the wider spectral coverage and higher spatial resolution of the new instruments with respect to GOME leading to a likely reduction in the uncertainties associated to the retrieval method.

## INTRODUCTION

Aerosols have direct and indirect influences on the atmospheric processes. Particles scatter and absorb solar radiation and enter cloud microphysical processes acting as cloud condensation nuclei. Certain type of aerosols can even affect the precipitation process, as it was recently confirmed [1], [2]. Moreover, the short lifetime of these particles causes high spatial and temporal variability of aerosol optical thickness and optical properties. Therefore, the characterization of single aerosol events as well as the establishment of its climatology require global observations with adequate time and space resolution.

Data from geostationary meteorological satellites (e.g. METEOSAT [3]) and polar orbiting instruments as NOAA-AVHRR [4], have been widely used for monitoring the AOT over the oceans. However, it is more and more clear that the understanding of the impact of aerosols on climate requires a correct determination of the aerosol spectral optical properties as well as of the AOT. This limits the use of such sensors for accurate aerosol quantification due to their wide spectral channels. On one hand, they do not allow for aerosol type characterization, constraining the algorithms to the use of aerosol classes available in the literature and thus introducing significant errors in the AOT calculations. On the other hand, it is difficult to account for the surface reflectance effect and atmospheric gases as is the case of ozone and especially water vapor.

The techniques for aerosol optical thickness retrieval and aerosol characterization and their accuracy strongly depend on the characteristics of the sensor as described in [5]. The GOME sensor [6] presents spectral characteristics suitable for the detection and characterization of the aerosol load in the atmosphere [7], [8]. Relevant shortcomings for an effective monitoring of aerosol events are, however, its low spatial and temporal resolution. The possible use of data from both polar (GOME) and geostationary (METEOSAT) satellite systems has already been exploited for the monitoring of large aerosol events over the ocean [9]. This kind of synergy aims at a better exploitation of the advantages of both kind of sensors and at the same time overcomes as much as possible their limitations.

In the following the novelties of the aforementioned algorithm are described for the derivation of aerosol spectral optical properties from the pseudo-inversion of selected GOME spectral measurements. A mathematical minimization method is introduced in order to fit the simulated spectra with a radiative transfer model to the correspondent measured ones. The retrieved aerosol characteristics are then used for the AOT calculation and monitoring; a test case is presented. Results are compared with space-time co-located AOT measurements from the ground-based sun-photometer network AERONET (Aerosol Robotic NETwork) and POLDER (POLarization and Directionality of Earth Reflectances) as a preliminary validation of the algorithm.

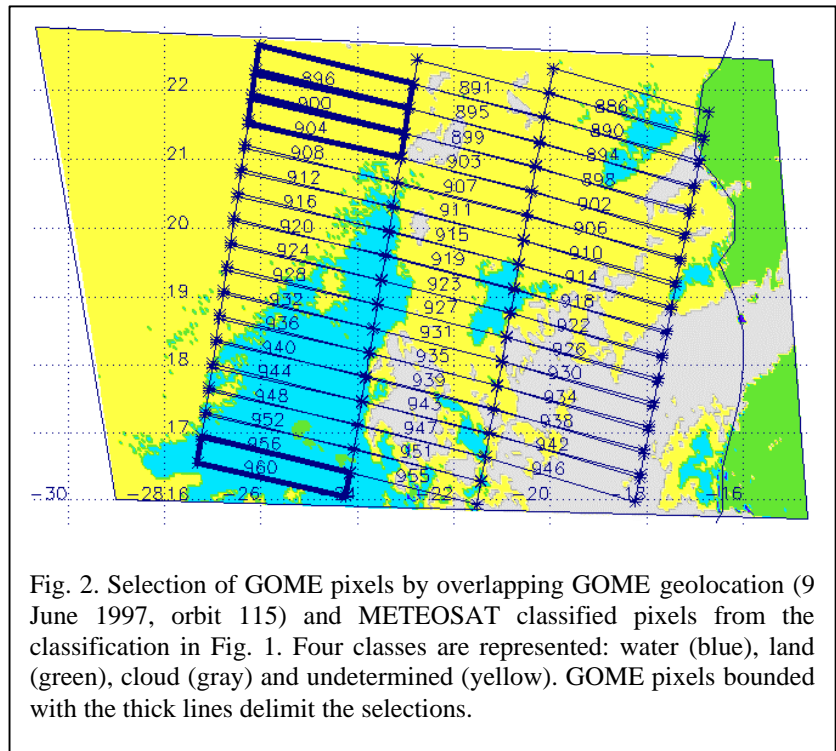
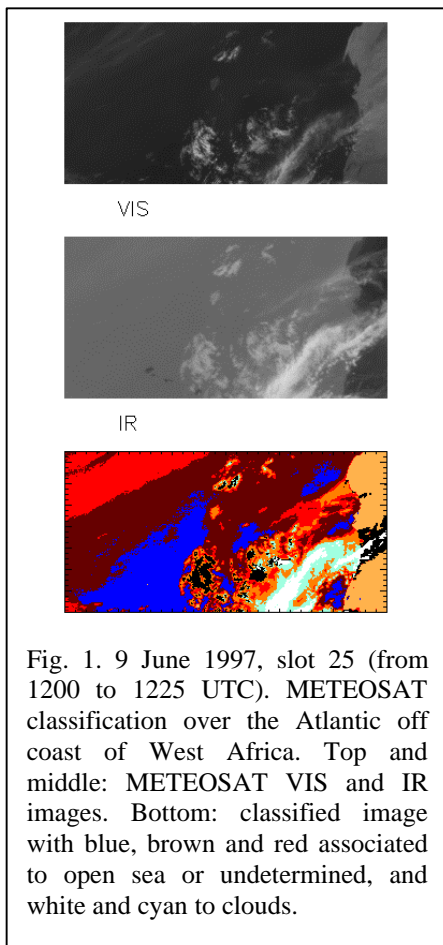
## AEROSOL TYPE CHARACTERIZATION ALGORITHM

The interaction of aerosols with solar radiation is characterized by their extinction and scattering coefficients, as well as phase function. The first two quantities describe the attenuation of radiation due to extinction (absorption and scattering) and scattering processes, respectively. The phase function in turns describes the angular distribution of the scattered radiation. The optical quantities are derived from micro-physical aerosol properties (such as the complex refractive index and the size distribution parameters) via the Mie theory assuming spherical particles. The aerosol size distribution and spectral refractive index are retrieved through a pseudo-inversion of GOME spectral measurements.

### Automated GOME Pixel Selection

The retrieval of aerosol properties requires GOME spectra be measured over cloud and land free regions that are horizontally homogeneous thus making the ground pixels selection essential. Matching GOME geo-location with METEOSAT best space-time coincident classified images is a practical way for a correct selection. METEOSAT scene classification is done using a statistical VIS-IR algorithm [10]. The method distinguishes several classes (water, land, broken cloud over water, broken cloud over land, cloud, and an undetermined class in case of problematic classification). Although the undetermined class can be due to the presence of very thin clouds, it is mostly connected with relevant aerosol transport events. Fig. 1 shows an example of the classification.

GOME geolocation is overlapped to METEOSAT classified pixels as in Fig. 2. METEOSAT's spatial resolution is  $5 \times 5 \text{ Km}^2$  at the nadir, whereas GOME's is  $320 \times 40 \text{ Km}^2$ : obviously, each GOME ground pixel encloses several METEOSAT pixels. GOME pixels are selected only when all the contained METEOSAT pixels are classified as water or as undetermined. The best possible space-time simultaneity of METEOSAT and GOME imagery is achieved using METEOSAT full-disk cuts nearest in time to the areas covered by GOME orbits. In the worst case, there is a time difference of 15 min between the two scans. A total of 145 pixels from 14 GOME orbits were selected between 5 and 11 June 1997 over the Atlantic Ocean within METEOSAT spatial coverage.



## Inversion Method

The pseudo-inversion of GOME selected reflectance spectra is done by fitting of GOME simulated reflectances to the corresponding measurements. Simulations are done at selected wavelengths ( $0.361, 0.421, 0.753$  and  $0.783 \mu\text{m}$ ) in order to avoid gas absorption as much as possible. The radiative transfer model used is 6S (Second Simulation of the Satellite Signal in the Solar Spectrum) [11], considering a tropical atmosphere since the case studied correspond to low-latitude regions and assuming a lambertian ocean surface. Aerosol is characterized by a bimodal log-normal size distribution composed by a fine and a coarse mode, both with the same spectral complex refractive index (parameters summarized in Table 1). The fitting process is repeated twice and the variation interval for each of the fitting parameters is also shown in Table 1. The free parameters of the first fitting process are the two modal radii and the imaginary refractive index in 2 different spectral regions (from about  $0.35$  to  $0.5 \mu\text{m}$  and  $0.7$  to  $0.86 \mu\text{m}$ ). On a second stage of the fitting, the AOT initialization value ( $\tau_a^*$ ) obtained as described in [7], is varied within a 30% limit, keeping fixed the best-fit parameters obtained in the first part of the process.

The mathematical method used for the fitting is the continuous minimization by simulated annealing. The method can be well suited for problems of finding the global extremum of a function in the presence of several local extrema. In the present case it is applied to the minimization of a function that describes the agreement between measurements and simulations. The algorithm requires four basic elements: the value of the function  $f(\mathbf{x})$  to be minimized, being  $\mathbf{x}$  a vector of  $M$  variables; the  $\mathbf{x}$  vector, i.e., the initialization values of the fitting parameters; a control parameter with a corresponding annealing schedule, to be gradually reduced; and a generator of random changes to calculate the next

step ( $\mathbf{x}$  to  $\mathbf{x}+\Delta\mathbf{x}$ ). The algorithm is implemented using a modified downhill simplex method with a suitable annealing schedule that allows for the efficient exploration of the variation interval of each parameter so that even in the presence of local minima it continues the search for the best (global) minimum. A full description of the algorithm can be found in [12].

The function  $\mathbf{f}(\mathbf{x})$  to be minimized is the well-known chi-square. Equations (1) and (2) correspond to the first and second part of the fitting process, respectively:

$$\mathbf{c}^2(R_F, R_C, \text{Im}_1, \text{Im}_2) = \sum_{i=1}^n \left( \frac{\mathbf{r}^G(\mathbf{l}_i) - \mathbf{r}^S(\mathbf{l}_i, \mathbf{t}_a^*; R_F, R_C, \text{Im}_1, \text{Im}_2)}{\mathbf{s}(\mathbf{l}_i)} \right)^2 \quad (1)$$

$$\mathbf{c}^2(\mathbf{t}_a) = \sum_{i=1}^n \left( \frac{\mathbf{r}^G(\mathbf{l}_i) - \mathbf{r}^S(\mathbf{l}_i, \mathbf{t}_a)}{\mathbf{s}(\mathbf{l}_i)} \right)^2 \quad (2)$$

where  $\tau_a^*$  is the AOT initialization value,  $R_F$  and  $R_C$  the modal radii of the fine and coarse mode, respectively,  $\text{Im}_1$  and  $\text{Im}_2$  the imaginary parts of the refractive index for the two aforementioned spectral regions, and  $\tau_a$  the AOT retrieved.  $\rho^G(\lambda_i)$  and  $\rho^S(\lambda_i)$  are the measured and simulated GOME spectral reflectances, respectively, and  $\sigma(\lambda_i)$  the standard deviations associated with GOME spectral measurements and  $n$  is the number of selected wavelengths  $\lambda_i$ .

Table 1. Size distribution and complex refractive index parameters. In bold are identified the lower and upper variation limits of the fitting parameters.

Mode	Modal radius (mm)	Standard Deviation	Percentage number density of particles	Spectral Complex Refractive Index	
				Spectral regions (mm)	
				0.35 – 0.50	0.70 – 0.86
Fine	<b>0.01-1.0</b>	2.5	0.999	1.48 – (0.0 – 0.05)i	1.48 – (0.0 – 0.01)i
Coarse	<b>0.5-10.0</b>	2.0	0.001		

Fig. 3 shows the fitting result corresponding to one of the selected GOME pixels. Also plotted for comparison are the same simulations using an aerosol class available in the literature [13], being the AOT the only fitting parameter. Note that there is a very good agreement between measurements and simulations for longer wavelengths, whereas the fixed aerosol model is unable to reproduce the measured reflectance at lower wavelengths.

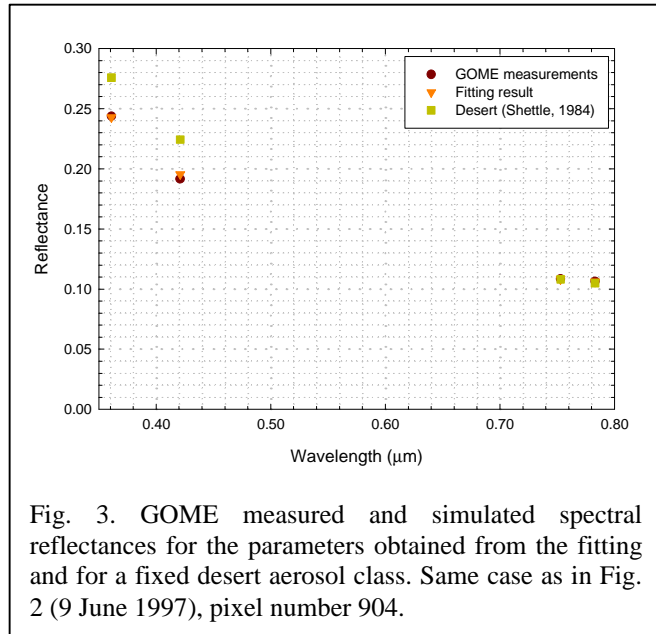


Fig. 3. GOME measured and simulated spectral reflectances for the parameters obtained from the fitting and for a fixed desert aerosol class. Same case as in Fig. 2 (9 June 1997), pixel number 904.

AOT values in this case were of 0.89 for the fitting result and 0.90 for the fixed aerosol model, while in other cases differences in AOT between them are much larger.

The inversion of each of the selected GOME spectral reflectances allows for the retrieval of several size distributions and complex refractive indexes that characterize the mixture of aerosol present in the atmosphere for each space-time measurement. Graphs in Fig. 4 show the scatter plots of the obtained fitting parameters. A cluster analysis [14] applied to these parameters correspondent to 70 inversions (high values of chi-square discarded) identified four classes represented in the plots by four different colors.

The four clusters from the analysis results in four mean size distributions and respective refractive indexes, all shown in Table 2.

Aerosol particles are assumed to be spherical and Mie theory is used to compute their spectral optical properties from the retrieved mean size distributions and spectral refractive indexes. The graphs in Fig.5-7 show

these properties at four of the 6S working wavelengths (0.400, 0.488, 0.694 and 0.860  $\mu\text{m}$ ), which are the nearest to the GOME wavelengths used in the fitting.

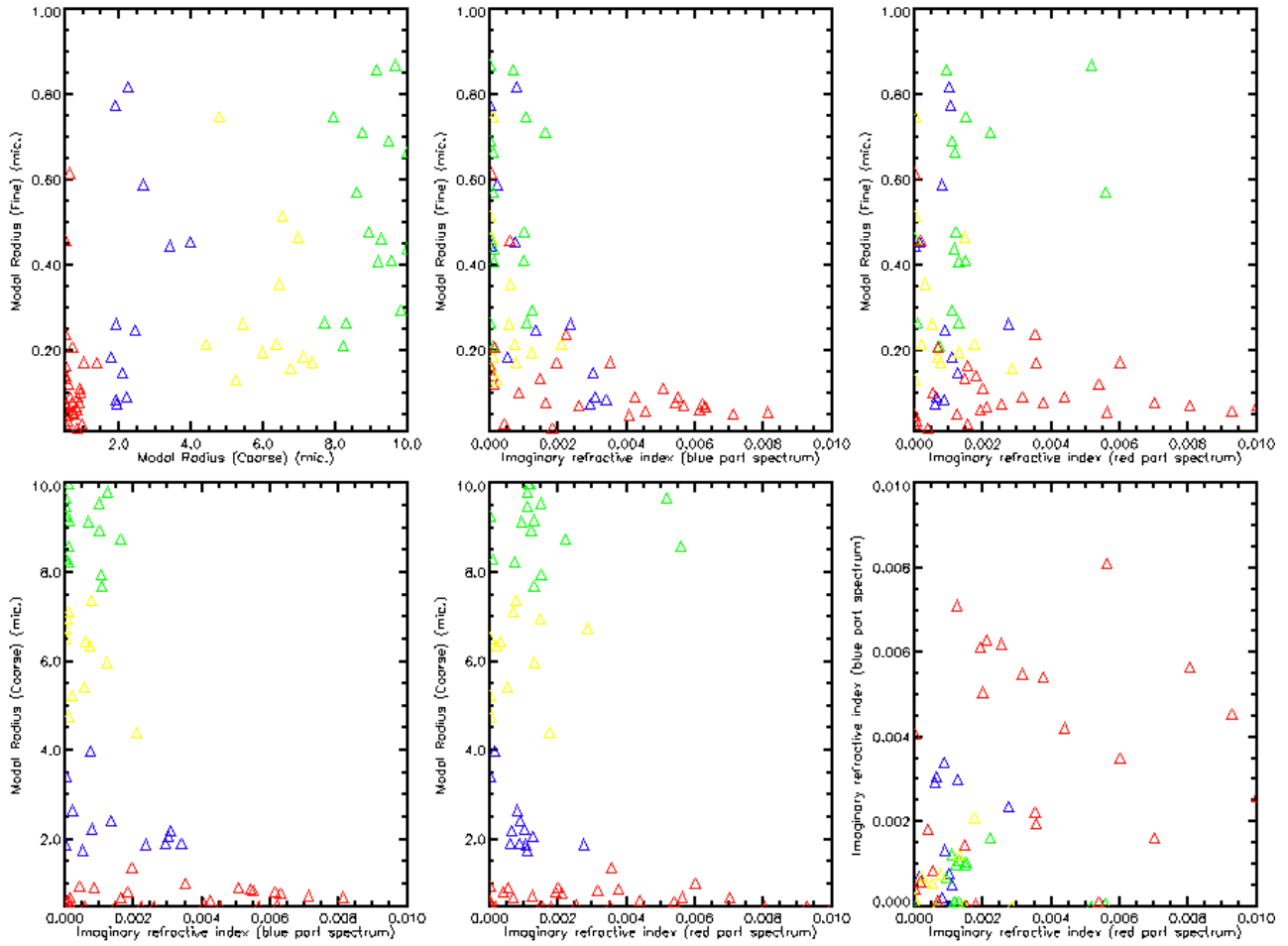
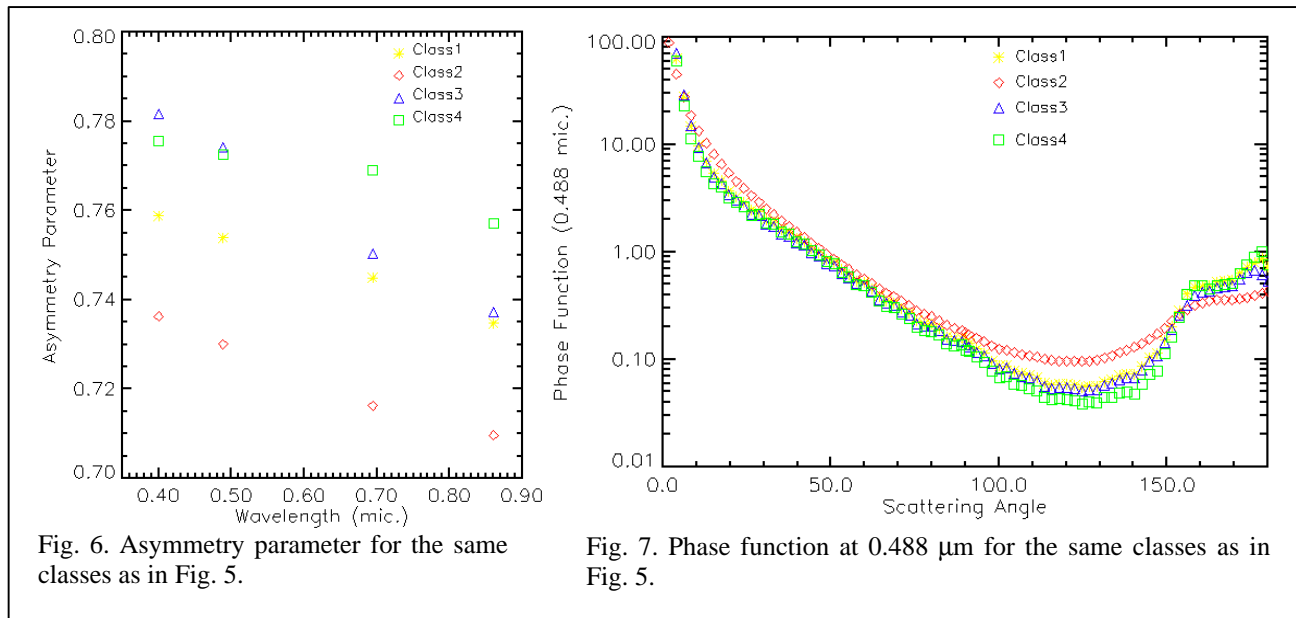
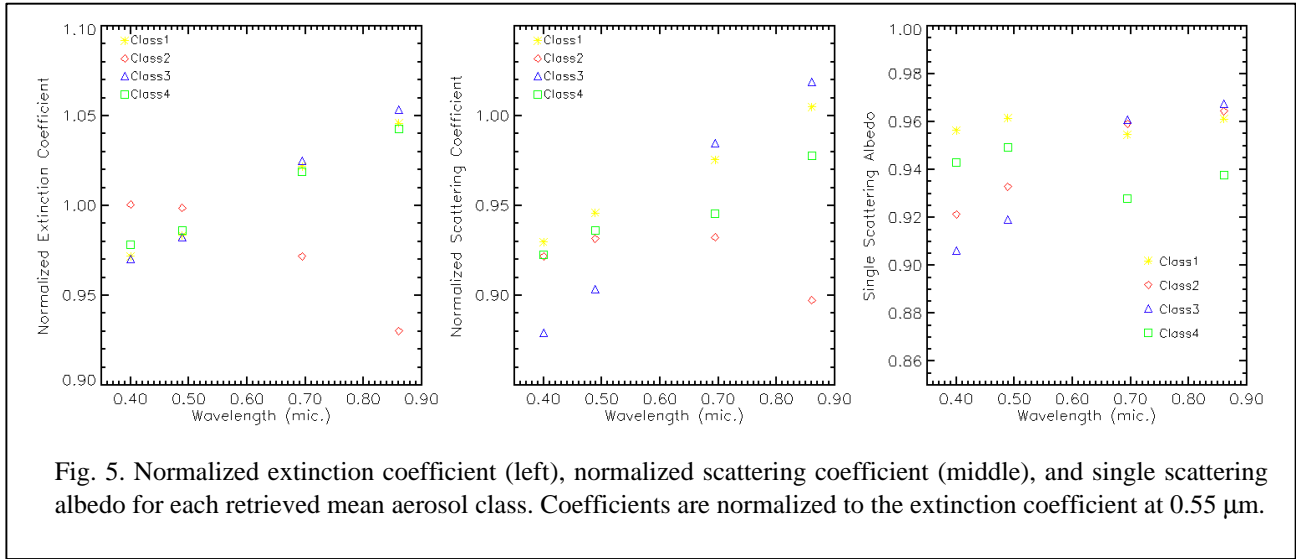


Fig. 4. Scatter plots of the size distribution parameters obtained from the fitting (modal radii of fine and coarse modes and imaginary refractive indexes for two the spectral regions). Colors represent the different classes identified by the cluster analysis.

Table 2. Mean size distributions and complex refractive indexes retrieved from the cluster analysis of the selected GOME spectral reflectance inversion. In bold are the mean retrieved parameters.

Class	Mode	Modal radius (mm)	Standard Deviation	Percentage number density of particles	Spectral Complex Refractive Index	
					Spectral regions (mm)	
					0.35 – 0.50	0.70 – 0.86
1	Fine	<b>0.30</b>	2.5	0.999	1.48 – <b>0.0005i</b>	1.48 – <b>0.0008i</b>
	Coarse	<b>6.10</b>	2.0	0.001		
2	Fine	<b>0.10</b>	2.5	0.999	1.48 – <b>0.004i</b>	1.48 – <b>0.003i</b>
	Coarse	<b>0.70</b>	2.0	0.001		
3	Fine	<b>0.35</b>	2.5	0.999	1.48 – <b>0.0015i</b>	1.48 – <b>0.0009i</b>
	Coarse	<b>2.40</b>	2.0	0.001		
4	Fine	<b>0.52</b>	2.5	0.999	1.48 – <b>0.0005i</b>	1.48 – <b>0.001i</b>
	Coarse	<b>9.00</b>	2.0	0.001		



## APPLICATION TO A CASE STUDY

GOME-derived aerosol classes are used to retrieve and monitor the AOT from METEOSAT-6 measurements over the Atlantic Ocean in the area represented in Fig.8, where a strong Saharan dust event occurred at the beginning of June 1997. Although the accuracy of METEOSAT-6 VIS measurements present some problems with respect to calibration and spectral response, it is demonstrated [15] that in most of the cases the use of GOME-derived aerosol classes instead of fixed climatological classes from literature makes a significant difference even considering large measurement errors (15%).

LookUp Tables (LUTs) of METEOSAT VIS radiance are built for 9 AOT values (0.0, 0.1, 0.2, 0.5, 1.0, 1.5, 2.0, 2.5, 3.0), as a function of the GOME-derived aerosol class (Table 2) and viewing geometry ( $2^\circ$  step in solar and satellite zenith angles). The METEOSAT radiance is simulated with the radiative transfer model 6S, considering a tropical

vertical profile of pressure, temperature, water vapor and ozone and a lambertian ocean surface, which can be considered reasonable approximations for the situation considered [15].

The LUT correspondent to each METEOSAT pixel is chosen according to the nearest viewing geometry and the aerosol class assigned to the nearest GOME pixel in time and space. Fig. 8 shows the AOT maps retrieved for the dust event studied.

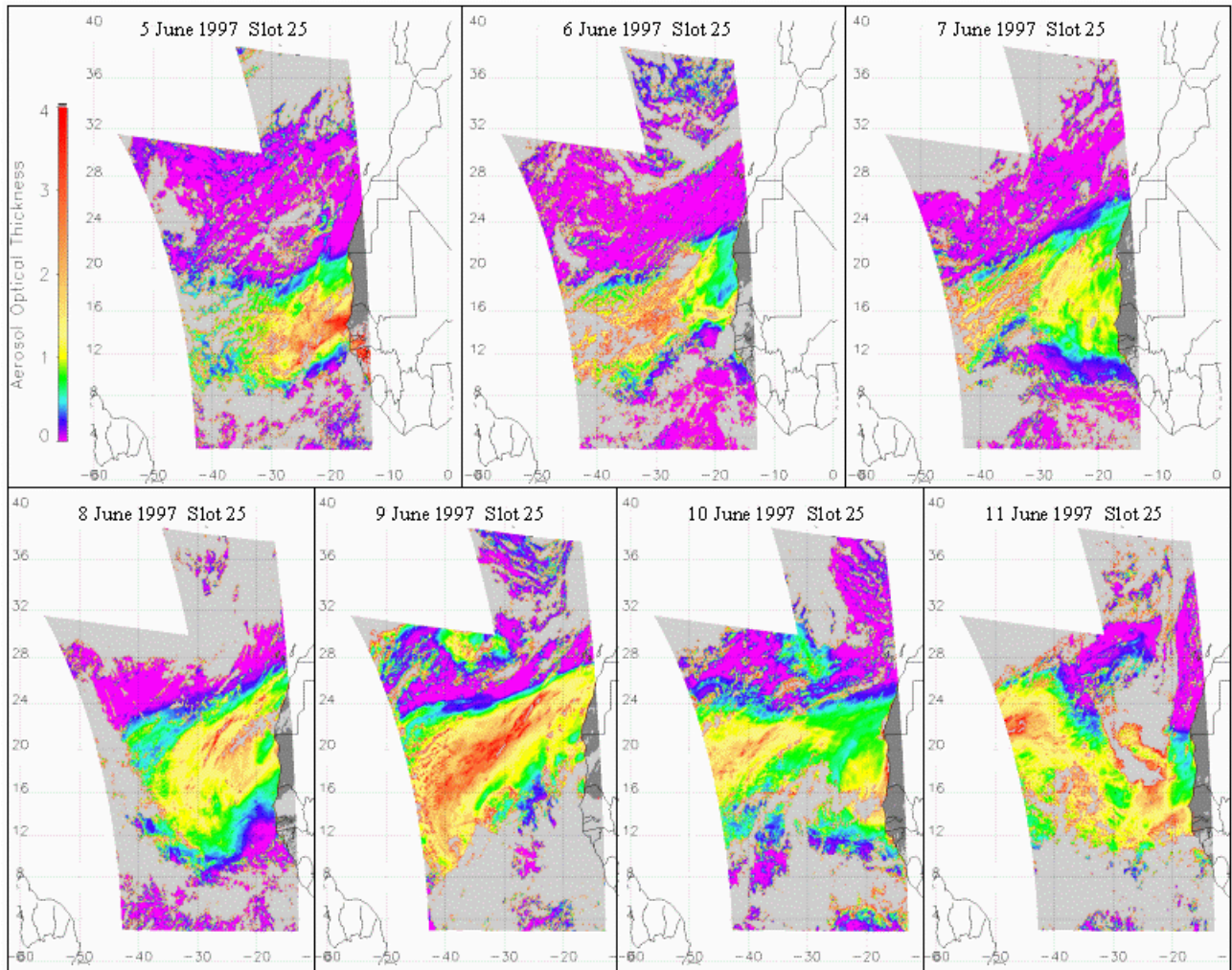


Fig. 8. 5 to 11 June 1997. AOT maps retrieved from METEOSAT-6 VIS radiance at slot 25, using the GOME-derived aerosol classes. Light gray is associated to cloudy pixels and dark gray to land.

## PRELIMINARY VALIDATION

The AOT values in Fig. 8 are compared with ground-based station measurements from AERONET, which maintains two sites in the area, Capo Verde and Dakar. The METEOSAT scans the area at about 1215 UTC; the AERONET measurements nearest in time are taken for the comparisons shown in Fig. 9. AOT values correspondent to the METEOSAT pixels located inside a  $0.4 \times 0.4^\circ$  box centered on the geographical location of the site are averaged. Vertical error bars refer to the standard deviation computed from the sample of AOT values inside the box. The AOT value correspondent to the spatially nearest METEOSAT pixel with respect to the measurement site is also plotted, as well as a comparative value obtained for the same pixel using a fixed desert aerosol class [13]. On each day the left symbols refer to Capo Verde, while the right ones to Dakar.

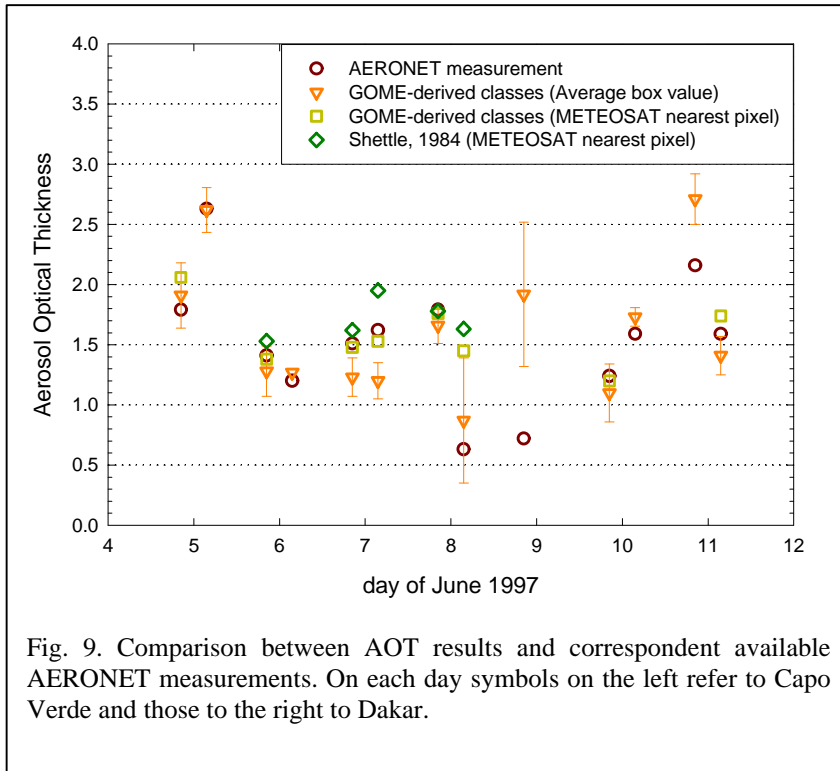


Fig. 9. Comparison between AOT results and correspondent available AERONET measurements. On each day symbols on the left refer to Capo Verde and those to the right to Dakar.

the AOT from both algorithms were computed for boxes of  $0.5^\circ \times 0.5^\circ$ , retaining only pixels with a correspondent AOT value lower than 3.0. The percentage of these pixels was calculated with respect to the total number of pixels located within the box; the cell is retained for comparison only if the value exceeds 40% (marked with the black box).

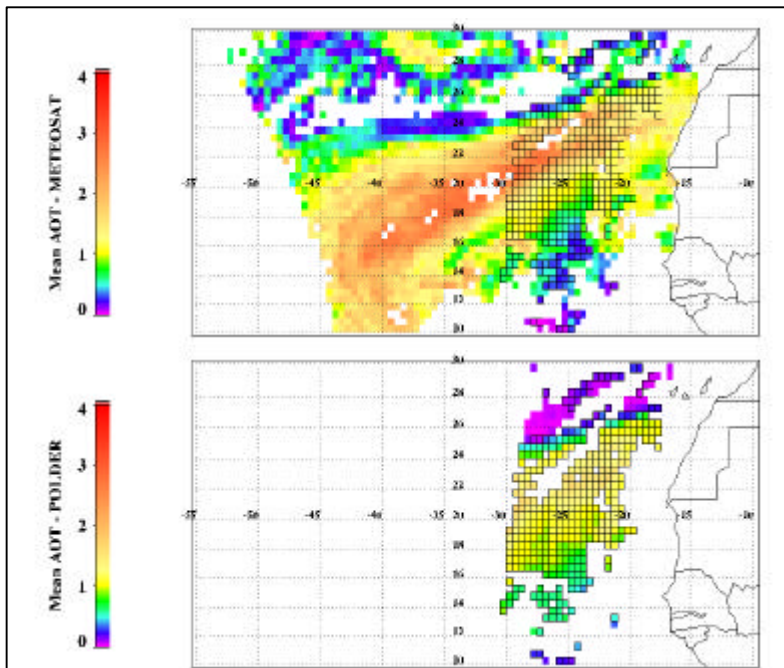


Fig. 10. 9 June 1997. Comparison between space-time coincident AOT results obtained with the present algorithm and AOT POLDER product. Pixels enclosed in the black boxes were retained for comparison.

The comparison shows a good agreement between AOT values retrieved with METEOSAT VIS data using GOME-derived aerosol classes and AERONET measurements for most of the cases. Although the comparison is done for a limited number of cases, note that these values better match the measurements than those obtained with the fixed aerosol class.

The disagreement for Capo Verde on 11 June 1997 might be related to the fact that the measurement was done at about 1100 UTC, more than one hour before METEOSAT's scan time. For the rest of the cases there was a maximum time difference of 10 min.

The AOT values in the maps of Fig. 8 were compared with the POLDER AOT product [16], for space-time best coincidence retrievals, over the area shown in Fig. 10. The example refers to 9 June 1997, but comparisons were also done for 5, 8 and 11 June 1997 with similar results. Mean values of

There is a good agreement between AOT results obtained with GOME-derived aerosol classes and POLDER AOT which is calculated in a total independent way. Greater differences for higher aerosol loads (Fig. 11) might be related to the fact that the POLDER AOT algorithm obtains these values by extrapolation and neglecting absorption [16].

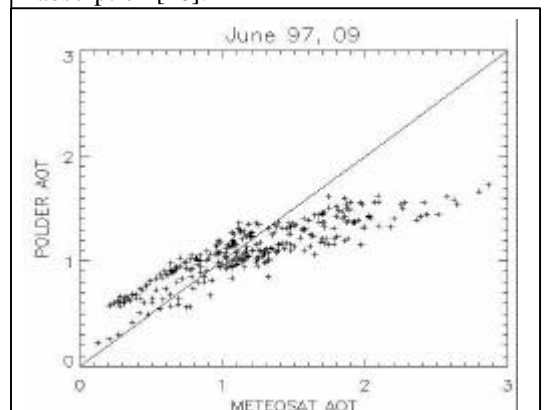


Fig. 11. Scatter plot of AOT results from METEOSAT and POLDER comparison of Fig. 10.

## DISCUSSION AND PERSPECTIVES

GOME high spectral resolution measurements are used to characterize the aerosol mixture present in the atmosphere over selected areas, in order to avoid the use of aerosol classes available in the literature and representative of mean atmospheric conditions. In spite the coarse spatial resolution of the sensor and the consequent assumption of using the same aerosol properties over a large geographical area, the errors introduced in AOT retrievals by the use of inadequate aerosol classes should be minimized.

The use of geostationary data for AOT retrievals gives the possibility of following the daily evolution of an aerosol event with a very good temporal resolution (30 min). A polar orbiting instrument can guarantee at most a few overpasses a day with obvious limitations in monitoring some features of the evolution of the event.

The proposed combination of data from sensors onboard polar and geostationary platforms aims at overcoming limitations from both types of satellite taking advantage of their respective strengths and thus contributing to an increasingly accurate aerosol characterization and continuous monitoring.

The comparison between AOT results from the present algorithm and simultaneous AERONET measurements reveals a good agreement for most of the cases. Moreover, the case study shows an improvement in the accuracy of AOT retrievals when using the GOME-derived aerosol classes with respect to a fixed aerosol class. In addition, comparisons with POLDER AOT product show a good agreement for the majority of the cases.

GOME offers high spectral resolution measurements, which undoubtedly represent important data to characterize atmospheric constituents. A future perspective with the launch of the three nadir viewing spectrometers onboard ENVISAT-1 (AATSR, MERIS and SCIAMACHY) looks very promising. The synergistic use of the three sensors will enlarge the present spectral coverage and provide a better spatial resolution with respect to GOME's, contributing to improve the detection and characterization of atmospheric aerosols [17], [18]. The introduction of such combined measurements in the present algorithm will certainly have positive effects in reducing uncertainties in the inversion method, since the additional spectral information is important for aerosol absorption and size distribution characterization; this information is also very useful for simultaneous cloud detection. The improvement in spatial resolution in turns will increase the number of selectable cloud-land free homogeneous pixels, thus improving the confidence on the retrieved mean aerosol classes.

## ACKNOWLEDGMENTS

METEOSAT imagery was kindly made available by EUMETSAT. The work was supported by Agenzia Spaziale Italiana (ASI) through contract *Sinergia GERB-SEVIRI nello Studio del Bilancio Radiativo a Scala Regionale e Locale* and European Space Agency (ESA-ESRIN) through contract *Improvement and Validation of the GASP Aerosol Product*. AERONET data are available at <http://aeronet.gsfc.nasa.gov:8080/> thanks to NASA, CNES and CNRS. POLDER aerosol parameters presented in this paper were obtained using data from CNES's POLDER onboard NASDA's ADEOS. MJC was financially supported by the *Subprograma Ciência e Tecnologia do 2º Quadro Comunitário de Apoio*.

## REFERENCES

- [1] D. Rosenfeld, "Suppression of rain and snow by urban and industrial air pollution", *Science*, vol. 287, pp. 1793-1796, March 2000.
- [2] D. Rosenfeld, "TRMM observed first direct evidence of smoke from forest fires inhibiting rainfall", *Geophys. Res. Lett.*, vol. 26, pp. 3105-3108, October 1999.

- [3] C. Moulin, F. Guillard, F. Dulac, and C. E. Lambert, "Long-term daily monitoring of Saharan dust load over ocean using METEOSAT ISCCP-B2 data: 1. Methodology and preliminary results for 1983-1994 in the Mediterranean", *J. Geophys. Res.*, vol. 102, pp 16,947-16,958, July 1997.
- [4] L. L. Stowe, A. M. Ignatov, and R. R. Singh, "Development, validation, and potential enhancements to the second-generation operational aerosol product at the National Environmental Satellite, Data, and Information Service of the National Oceanic and Atmospheric Administration", *J. Geophys. Res.*, vol. 102, pp 16,923-16,934, July 1997.
- [5] M. King, Y. Kaufman, D. Tanré, and T. Nakajima, "Remote sensing of tropospheric aerosols from space: Past, present, and future", *Bull. Am. Meteor. Soc.*, vol. 80, pp. 2229-2259, November 1999.
- [6] J. P. Burrows, M. Weber, M. Buchwitz, V. Rozanov, A. Ladstätter-Weißmeyer, A. Richter, R. DeBeek, R. Hoogen, K. Bramstedt, K.-U. Eichmann, and M. Eisinger, "The Global Ozone Monitoring Experiment (GOME): Mission concept and first scientific results", *J. Atmos. Sci.*, vol. 56, pp. 151-175, January 1999.
- [7] F. Torricella, E. Cattani, M. Cervino, R. Guzzi, and C. Levoni, "Retrieval of aerosol properties over the ocean using GOME measurements: Method and applications to test cases", *J. Geophys. Res.*, vol. 104, pp 12,085-12,098, May 1999.
- [8] A. Bartoloni, P. Colandrea, R. Loizzo, M. Mochi, F. Pascuali, N. Santantonio, E. Zappitelli, and M. Cervino, "SYSGOME: Processing chain for aerosol optical thickness product generation at I-PAF", *Proc. 2000 EUMETSAT Meteorological Satellite Data Users' Conf.*, pp. 460-467, May 2000.
- [9] M. J. Costa, M. Cervino, E. Cattani, F. Torricella, V. Levizzani, and A. M. Silva, "Aerosol optical thickness and classification: use of METEOSAT, GOME, and modelled data", *Proc. SPIE: Satellite Remote Sensing of Clouds and the Atmosphere IV*, J. E. Russell Ed., vol. 3867, pp. 268-279, September 1999.
- [10] F. Porcú, and V. Levizzani, "Cloud classification using METEOSAT VIS-IR imagery", *Int. J. Remote Sensing*, vol. 13, pp 893-909, March 1992.
- [11] E. F. Vermote, D. Tanré, J.-L. Deuze, M. Herman, and J.-J. Morcrette, "Second simulation of the satellite signal in the solar spectrum: An overview", *IEEE Trans. Geosci. Remote Sensing*, vol. 35, pp. 675-686, May 1997.
- [12] W. H. Press, S. A. Teukolsky, W. T. Vetterling, and B. P. Flannery, *Numerical Recipes in Fortran 77*, 2<sup>nd</sup> ed., vol. 1. Cambridge University Press, pp. 436-448, 1997.
- [13] E. P. Shettle, "Optical and radiative properties of a desert aerosol model", *International Radiation Symposium (IRS): Current problems in atmospheric radiation*, G. Fiocco Ed., pp. 74-77, A. Deepak, Hampton, Va., 1984.
- [14] IDL, *Reference Guide, Version 5.1*, Research Systems, Inc., Boulder, CO, 1998.
- [15] M. J. Costa, M. Cervino, E. Cattani, F. Torricella, V. Levizzani, and A. M. Silva, "An update of a GOME-METEOSAT method for aerosol optical thickness determination and classification", *Proc. 2000 EUMETSAT Meteorological Satellite Data Users' Conf.*, pp. 420-427, May 2000.
- [16] P. Goloub, D. Tanré, J.L. Deuzé, M. Herman, A. Marchand, and F-M. Bréon, "Validation of the first algorithm for deriving the aerosol properties over the ocean using the POLDER/ADEOS measurements", *IEEE Trans. Geosci. Remote Sensing*, vol. 37, pp. 1586-1596, May 1999.
- [17] F. Torricella, E. Cattani, M. Cervino, M. J. Costa, and V. Levizzani, "Detection and characterisation of atmospheric aerosol using simulated measurements from ENVISAT-1 nadir viewing spectrometers", *Proc. 2000 EUMETSAT Meteorological Satellite Data Users' Conf.*, pp. 428-435, May 2000.
- [18] M. Cervino, E. Cattani, F. Torricella, M. Mochi, D. Cerchia, P. Colandrea, M. Silvestri, and L. De Fusco, "Synergistic use of MERIS and SCIAMACHY instruments on board of ENVISAT-1: a test case with simulated data", *Proc. 2000 EUMETSAT Meteorological Satellite Data Users' Conf.*, pp. 436-442, May 2000.